Fish and Shellfish Immunology 91 (2019) 159–171

Contents lists available at ScienceDirect

Fish and Shellfish Immunology

journal homepage: www.elsevier.com/locate/fsi

Full length article

Immune and xenobiotic responses of glutathione S-Transferase theta (GST-θ) from marine invertebrate disk abalone (*Haliotis discus discus)*: With molecular characterization and functional analysis

W.M. Gayashani Sandamalika, Thanthrige Thiunuwan Priyathilaka, Seongdo Lee, Hyerim Yang, Jehee Lee*

Department of Marine Life Sciences & Fish Vaccine Research Center, Jeju National University, Jeju Self-Governing Province, 63243, Republic of Korea

ARTICLE INFO

Keywords:
Glutathione s-transferase theta (*GST-θ*)
Disk abalone (*Haliotis discus discus*)
Immune challenge
mRNA expression profile
Detoxification

ABSTRACT

Representing a multifunctional complex group of proteins, glutathione S- transferases (GSTs) play a major role in the phase II detoxification process in a wide range of organisms. This study focused on the potential detoxification ability of disk abalone (*Haliotis discus discus*) GST theta (*AbGST-θ*) under different stress conditions with special reference to post immune challenges. Characterization of AbGST-θ revealed with 226 amino acids, 26.6 kDa of predicted molecular mass and 8.9 of theoretical isoelectric point. As illustrated in the multiple sequence alignment, eight glutathione binding sites (G-sites) and ten substrate binding sites (H-sites) were identified in well-distinct N-terminal and C-terminal domains of AbGST-θ, respectively. AbGST-θ exhibited its highest sequence identity with *Mizuhopecten yessoensis* (59.1%) and the phylogenetic tree clearly positioned AbGST-θ with pre-defined GST-θ molluscan homologues. The *AbGST-θ* was highly expressed in the digestive tract of un-challenged abalones. Upon administering the challenge experiment, *AbGST-θ* showed significant modulations in their transcriptional levels depending on the time and the tissue type. The optimum temperature was 37 °C and optimum pH was 7.5 for AbGST-θ. The determined enzyme kinetic parameters of AbGST-θ showed low affinity towards 1-Chloro-2,4-dinitrobenzene (CDNB) and glutathione (GSH) as substrates. Nonetheless, with Cibacron blue IC_{50} (half maximal inhibitory concentration) was calculated to be 0.08 μM while observing 100% inhibition with 100 μM. Furthermore, AbGST-θ resulted in significant protection ability towards H_2O_2, $CdCl_2$, and $ZnCl_2$ in the disk diffusion assay. Collectively, this study provides evidences for the detoxification ability and the immunological host defensive capability of *AbGST-θ* in disk abalone.

1. Introduction

All the chemical reactions interacting with xenobiotic metabolism can be divided in to two main phases as phase I and phase II [1]. The phase II reactions have the ability to form complexes with their parent chemical or its metabolites, engaging with endogenous substrates which finally convert the initial lipophilic compound in to an inactive hydrophilic form [1]. Conjugation with glutathione (GSH) is considered one of the most important routes of metabolism, which protects the cells by detoxication of reactive metabolites [2]. This reaction is catalyzed by the glutathione S-transferase (GST) enzymes which are localized in cytosol and the endoplasmic reticulum [2]. Glutathione S-transferase has been identified as a superfamily of isoenzymes appearing in various organisms including mammals, birds, fish, plants, insects, and microbes [3]. Apart from the catalytic functions, these enzymes have also exhibited non-catalytic functions such as the modulation of signal transduction pathways, intracellular transportation of hydrophobic ligands, and sequestering carcinogens [3]. GSTs are categorized in to three main groups based on the homology of the amino acid sequence and the structure: cytosolic, mitochondrial, and MAPEG (membrane-associated proteins involved in eicosanoid and glutathione metabolism) GSTs [4]. Mitochondrial GST is a group of soluble enzymes, referred to as Kappa class GSTs, which share structural similarities with cytosolic GSTs. On the other hand, MAPEG are membrane associated proteins which express evolutionary distal with the other classes [5]. The cytosolic GSTs are a widely spread group which has further divided in to thirteen different classes based on their N-terminal amino acid sequence, substrate specificity, effective inhibitors, and

* Corresponding author. Marine Molecular Genetics Lab, Department of Marine Life Sciences, Jeju National University, Jeju Self-Governing Province, 63243, Republic of Korea.
E-mail address: jehee@jejunu.ac.kr (J. Lee).

https://doi.org/10.1016/j.fsi.2019.04.004
Received 29 November 2018; Received in revised form 25 March 2019; Accepted 2 April 2019
Available online 12 May 2019
1050-4648/ © 2019 Elsevier Ltd. All rights reserved.

cross reactions over the antibodies as: Alpha (α), beta (β), delta (δ), kappa (κ), sigma (σ), theta (θ), mu (μ), omega (Ω), pi (π), tau (τ), zeta (ζ), phi (ϕ), and epsilon (ε) [6]. Cytosolic GSTs can be identified as homodimers or heterodimers consisting of two distinct domains of 23–30 kDa in each monomer as: An thioredoxin-like domain at the N-terminal and an alpha helical domain a the C-terminal [7]. The dimer interface may have variations as hydrophobic ball-and-socket (α, μ, π, ϕ classes) or hydrophilic nature (θ, σ, β, classes). The thioredoxin-like domain is responsible for GSH binding with a specific substrate, hence termed as GSH-binding sites (G-site) [5]. The catalytic activity of these G-sites are controlled by tyrosine (Tyr), serine (Ser), or cysteine (Cyst) residues, considered as critical mediators of glutathione conjugation [8]. The C-terminal domain together with the N-terminal domain are involve in the shaping of hydrophobic substrate binding sites (H-site) [5]. Although the G-site sequences are highly conserved among the GST classes, H-sites have exhibited significant variations in their sequences, which allows the diversification of the substrate specificity [8].

GST theta (θ) class was first identified and characterized using 1-menaphthyl sulphate and 1,2-epoxy-3-(ρ-nitrophenoxy) propane as substrates [9]. However, GST-θ is considered the most ancient group which consists of two different types: GST-θ1 and GST-θ2 sharing 55% sequence identity in their protein structure. According to the studies of rats, although GSTs express an organ-specific pattern in their tissue distribution, most of the examined GST-θ were observed in the liver, lungs, blood, kidney, spleen, brain, testis, ovary, heart, and small intestine [6]. In human studies, GST-θ1 and GST-θ2 have been identified, cloned, and provided evidence for their ability to detoxify carcinogenic chemicals and chemotherapeutic agents [10]. To date, in marine invertebrates GST-θ has been characterized from freshwater prawns (*Macrobrachium rosenbergii*) [4], manila clams (*Ruditapes philippinarum*) [11], and sea cucumbers (*Apostichopus japonicus*) [12]. Of these, only the studies of GST-θ from manila clam and sea cucumber are consistent with the recombinant protein expression and functional studies. Moreover, apart from the xenobiotic detoxification of GSTs, these studies have further revealed the innate immune responses of GST-θ class by inducing the organisms with viral and bacterial pathogens.

Abalones are the most primitive gastropod mollusks living in the marine intertidal zone [13]. Being slow moving animals, they are highly vulnerable to contact with different types of natural xenobiotics from food sources, defensive toxins from other animals, and predator attacks [14]. Additionally, several other xenobiotic sources are present in the marine environment due to industrial and human anthropogenic activities [14], which can be potential toxins to marine organisms. The detoxification and elimination of these xenobiotics from organisms is essential for their survival, thus they possess diverse and numerous efficient enzymes which are involved in xenobiotic detoxification [14]. During the last few decades, abalones have been identified as highly susceptible for pathogenic invasions [13] such as *Vibrio parahaemolyticus* [15–18], *Vibrio harveyi* [19,20] and *Vibrio alginolyticus* [21] along with global factors including environmental pollution and climate change [22,23]. Mass mortalities in worldwide abalone farming contributed to great economic loss in the aquaculture industry, due to harmful pathogens and various diseases [13]. Lack of information regarding the molecular aspects and functional mechanisms of abalone immunity has become a major restriction on improving disease control strategies for abalone culture [24]. No evidence has been discovered in the literature for the GST- θ class of abalones in understanding its roles in immunity and functional perspectives. Therefore, in this study we discovered GST-θ from disk abalone (*Haliotis discus discus*), referred to as AbGST-θ, by revealing its host defensive biological functions over pathogenic and oxidative stress.

2. Materials and methods

2.1. Chemicals & reagents

For molecular experiments, Taq polymerase, SYBR Premix Ex Taq ™, and restriction enzymes were purchased from TaKaRa Bio, Japan. For the total RNA extraction, Tri Reagent™ (Sigma -Aldrich, USA) was used and the molecular markers were purchased from the Enzynomics, Korea. To challenge the abalones, purified Lipopolysaccharide (LPS) from *Escherichia coli* (055: B5; Sigma -Aldrich, USA) and polyinosinic: polycytidylic acid (poly (I: C)) (Sigma -Aldrich, USA) were used as immune stimulants. Reduced glutathione (GSH), 1-chloro-2,4-dinitrobenzene (CDNB), 1,2- dichloro-4-nitrobenzene (DCNB), ethacrynic acid (ECA), 4-nitrobenzyl chloride (4-NBC), and 4-nitrophenethyl bromide (4-NPB) were purchased from Sigma-Aldrich. Cibacron blue (CB) and isopropyl-β-D-thiogalactopyranoside (IPTG) were purchased from Polyscience Inc and Promega, respectively.

2.2. Experimental animals

Healthy disk abalones with 50 ± 5 g of an average body weight and 8 cm of an average shell length were purchased from a commercial abalone hatchery in Jeju Island, Republic of Korea. Abalone acclimatization to the laboratory conditions was proceeded one week prior to the experiment. During the acclimatization period, abalones were maintained in 60 L flat-bottomed fiberglass tanks with aerated sea water. The temperature was maintained at 20 ± 1 °C and the salinity was maintained at 34 ± 0.6 psμ. A daily diet of *Undaria pinnatifida* (10% of body weight), a kind of sea weed, was given as food for abalones.

2.3. Identification of AbGST-θ and bioinformatics analysis

The full-length coding sequence (CDS) for *H. discus discus GST-θ* was identified using the abalone transcriptome database previously established in our laboratory [25] by using a Roche 454 Genome sequencer FLX system (GS-FLX™) [26]. As a summary, total RNA was extracted from healthy disk abalone tissues (mantle, hepatopancreas, muscle, digestive tract, gills, and head) using Tri Reagent™ (Sigma- Aldrich, Missouri, USA) and further processing was carried out with a FastTrack 2.0 mRNA isolation kit (Invitrogen, USA). To synthesize the first strand of cDNA, a Creator™ SMART™ cDNA library construction kit (Clontech, USA) was used, and the normalization was completed using a Trimmer cDNA normalization kit (Evrogen, Russia). The data obtained from the sequencing library with the Roche 454 platform and GS-FLX™ technology (DNA Link, Inc.) was used for the construction of a shotgun transcriptome database. The Basic Local Alignment Search Tool (BLAST) at the National Center for Biotechnology Information (NCBI) (http://www.ncbi.nlm.nih.gov/BLAST) was used to confirm the identity of the gene of interest, and it was defined as *AbGST-θ,* a homologue to earlier defined *GST-θ* genes. Using the ORF finder (https://www.ncbi.nlm.nih.gov/orffinder) web-based tool, the open reading frame (ORF) and corresponding amino acid sequence of the deduced protein was determined. For the identification of conserved domains and signal peptides in the *GST-θ*, ExPASy prosite [27] and SignalP [28] programs were used respectively. The SMART online server (http://smartembl-heidelberg.de) and NCBI-conserved domain database (CDD) (www.ncbi.nlm.nih.gov/Structure/cdd/cdd.shtml) were used for further analysis of the *GST-θ* profile. For the construction of the phylogenetic tree, MEGA 6 program was used based on the neighbor-joining method [29]. To determine the multiple sequence alignment, Clustal omega (http://www.ebi.ac.uk/Tools/msa/clustalo) [30] and color align conservation (http://www.bioinformatics.org/sms2/color_align_cons.html) [31] web based software was used. The three-dimensional (3D) model of GST-θ was determined through the use of SWISS-MODEL (https://swissmodel.expasy.org) protein structure modelling server [32], and the visualizing

was completed with PyMOL v1.5 software [33].

2.4. Tissue isolation for analysis of AbGST-θ expression in different tissues

Five healthy disk abalones were dissected and the gill, mantle, digestive tract, muscles, and hepatopancreas were carefully isolated to analyze the differential distribution of AbGST-θ in various abalone tissues. Before dissecting the abalone, after disinfecting with alcohol, hemocytes were obtained immediately from the pericardial cavity using a sterilized syringe. After that the cells were harvested by centrifugation at 3000 × *g* for 10 min at 4 °C. All the obtained tissue samples were snap-frozen and stored at −80 °C prior to RNA extraction.

2.5. Immune challenge experiment

To evaluate the immune responses of *AbGST-θ,* healthy disk abalones were divided into four groups (each group containing 30 individuals) and challenged with different bacterial and viral immune stimulants. One group of abalones were injected with *Vibrio parahaemolyticus* (KCTC2729); Gram-negative bacterial strain, obtained from the Korean collection for Type cultures. Briefly, it was cultured on LB marine plates by incubating at 25 °C overnight. A single colony was picked up and inoculated in 4 mL of marine broth and shaken at 25 °C for 16 h at 200 rpm. Then 1.5 mL of bacterial culture was centrifuged at 7000 g × at 4 °C for 5 min. After that the supernatant fluid was removed and the bacterial pellet was resuspended in sterile saline (0.9% NaCl) and it was serially diluted by measuring the cell density at 600 nm absorbance. Each abalone from the group was injected intramuscularly with live *V. parahaemolyticus* (100 μL, 1 × 10^4 CFU/μL). Another group of abalones was injected intramuscularly with 100 μL of double stranded RNA viral mimic poly I:C (5 μg/μL) to determine the immune responses of *AbGST-θ* over viral stimulants. One from the remaining two groups was injected intramuscularly with 100 μL of LPS (5 μg/μL, from *Escherichia coli* 055: B5; Sigma, St. Louis, MO, USA) in sterile saline. Each abalone in the final group was injected with 100 μL of sterile saline and were treated as the control group. After challenging the abalones, a total of four animals from each group were dissected at 3, 6, 12, 24, 48, 72, and 120 h post-injection (p.i.), and gill and hemocytes were collected from them as described in above section. All the collected tissue samples were snap-frozen in liquid nitrogen and stored at −80 °C until further dealing out.

2.6. Total RNA extraction & cDNA synthesis

From the collected tissue samples of healthy and challenged abalones, total RNA was extracted using TRIzol Reagent (Sigma) as per manufacturer's instructions. The RNA concentrations were determined spectrophotometrically, based on the absorbance at 260 nm (BioRad, USA). An aliquot (2.5 μg) of purified RNA sample (1 μg/μL) was used to synthesize the cDNA with the use of Prime Script™ first-strand cDNA synthesis kit (TaKaRa, Japan) according to vendor's recommendations. After that, the synthesized cDNA was diluted 40-fold and stored at −20 °C until use in further analysis.

2.7. AbGST-θ – Transcriptional profiling by quantitative real-time PCR

The transcriptional analysis was performed through quantitative real time PCR (qPCR) using a Real Time System TP800 Thermal Cycler Dice ™ (TaKaRa, Japan). During the process, SYBR Green was used as the fluorescent agent and all the steps were performed following Minimum Information for publication of Quantitative real-time PCR Experiments (MIQE) guidelines [34]. For the normalization of the *AbGST-θ* transcription, the abalone ribosomal protein L5 (GenBank accession: EF103443) was selected as the internal control gene [35]. Forward and reverse gene specific primers were designed for AbGST-θ and abalone ribosomal protein L5 (Table 1) and were used for the amplification of the products. The qPCR reaction mixture was prepared including 3 μL of diluted cDNA from appropriate tissue, 5 μL of 2 × TaKaRa Ex Taq™ SYBR premix, 0.5 μL of each forward and reverse primer (10 pmol/μL), and 1 μL of PCR grade dH_2O with a total volume of 10 μL. The PCR program performed with one cycle at 95 °C for 10 s; followed by 45 cycles of 95 °C for 5 s, 58 °C for 20 s; and 72 °C for 20 s; and a final single cycle of 95 °C for 15 s, 60 °C for 30 s, and 95 °C for 15 s. Obtained C_t values were subjected to calculate the relative mRNA expression levels using Livak ($2^{-\Delta\Delta CT}$) method [36]. All the immune challenged samples were normalized to the corresponding saline control at each time point. The mRNA expression at 0 h un-injected control was used as the basal level reference, and it was used to represent the results as fold changes (mean ± standard deviation).

2.8. Construction of expression plasmids

Cloning primers were designed with the EcoRI and SalI restriction sites (Table 1) to amplify the predicted CDS of *AbGST-θ*. PCR amplification was performed using a TaKaRa thermal cycler (Japan), and the ExTaq™ DNA polymerase (TaKaRa, Bio Inc., Japan). The reaction mixture was prepared with a total volume of 50 μL, containing 0.2 μL of *Ex Taq* polymerase (5 units/μL), 5 μL of 10 × *Ex Taq* buffer, 4 μL of 2.5 mM dNTPs, 5 μL of template cDNA, 1 μL of each primer (10 pmol/μL) and sterilized distilled water (PCR grade). The PCR profile was designed as follows, with an initial denaturation of 94 °C for 3 min; 35 cycles of amplification at 94 °C for 30 s, 59 °C for 30 s, and 72 °C for 1.5 min; and a final extension at 72 °C for 5 min. Amplified products were purified and allowed for the restriction digestion along with pMAL-c2X (New England Biolabs Inc, USA) vector using EcoRI and SalI restriction enzymes. The purified digested products were ligated using Mighty Mix (TaKaRa, Japan) at 4 °C overnight to produce the pMAL-c2X/*AbGST-θ* construct. It was then transformed in to *Escherichia coli* DH5α and the in-frame insertion was confirmed through sequencing.

2.9. Overexpression and recombinant protein purification

For the overexpression of recombinant AbGST-θ protein (rAbGST-θ), the pMAL-c2X/*AbGST-θ* construct was transformed in to *E. coli* BL21 (DE3) (New England BioLabs, USA). A seed culture was propagated from a single colony and it was transferred in to 250 mL of LB rich medium containing 0.2% of glucose and 100 μg/mL ampicillin and incubated at 37 °C until obtaining optical density of 0.6 at 600 nm (OD_{600}). At this point, Isopropyl-β-galactoside (IPTG) was added to the culture by maintaining 0.5 mM of final concentration, and further incubated in the shaking incubator at 200 rpm for 8 h at 20 °C to induce the protein expression. Thereafter, cells were harvested by centrifugation at 1200 × *g* for 30 min at 4 °C. Using column buffer (20 mM Tris-HCl, pH 7.4, 200 mM NaCl) the bacterial pellet was resuspended and stored at −20 °C for overnight.

Next, cells were thawed and Lysozyme (1 mg/mL) was added to lyse the cells together with cold sonication. The lysate was centrifuged at 9000 × *g* for 30 min at 4 °C. The rAbGST-θ protein was purified from the resultant crude extract by following maltose affinity chromatography, as described previously [37]. Maltose Binding Protein (MBP) was also purified repeating the same protocol. Using the Bradford method [38] the amount of protein in each fraction was determined and the approximate molecular mass of rAbGST-θ was estimated on 12% SDS-PAGE together with molecular standards (Enzynomics™, Korea).

2.10. Analysis of biochemical properties of rAbGST-θ

The specific activities of rAbGST-θ were determined as described previously [39]. The 200 μL of reaction mixture was maintained with 0.1 M phosphate buffer (pH 6.5), 100 mM reduced GSH, 100 mM substrate and an appropriate amount of rAbGST-θ. Different substrates were used for the initiation of the reaction as: CDNB, DCNB, 4-NPB, 4-

Table 1
Sequences of primers used in this study.

Primer name	Application	Sequence of primer (5′-3′)
AbGST-θ _F	ORF amplification	GAGAGAGAATTCATGGCGTTGAAAGTGTACTATGATTTGATGTCTC
AbGST-θ_R		GAGAGAGTCGACTCAAAGATTAGATCCAAGTGAGGACTTGGTCA
AbGST-θ_qF	qPCR	AACTGGCAGCACCTGAACACAAG
AbGST-θ_qR		TACCGGTGACAGCTTTACGAACCA
AbRib_F	qPCR Internal control	TCACCAACAAGGACATCATTTGTC
AbRib_R		CAGGAGGAGTCCAGTGCAGTATG

Table 2
Pairwise identity (I%), similarity (S%), and gaps (G%) of disk abalone GST-θ protein toward selected orthologs at amino acid levels.

Name	Accession no	Identity (%)	Similarity (%)	Gaps (%)	Amino acids
Mizuhopecten yessoensis	XP_021358629.1	59.1	75.3	2.1	235
Lingula anatina	XP_013408169.1	53.2	69.3	1.7	231
Alitta succinea	ABQ82132.1	49.4	69.3	2.6	231
Osmerus mordax	ACO09513.1	45.7	64.5	4.3	234
Danio rerio	NP_956815.2	44.4	61.5	4.3	234
Ruditapes philippinarum	AFB83399.1	39.9	59.3	14.1	248
Cephus cinctus	XP_015598273.2	39.6	54.9	15.7	255
Mus musculus	CAA66666.1	35.6	53.8	12.6	253
Macaca mulatta	NP_001244563.1	34.9	54.9	14.1	255
Homo sapiens	AAC13317.1	34.1	53.3	14.9	255

NBC, and ECA. Absorbance of the reactions were determined at the corresponding wave lengths (Table 2), immediately, and after 5 min while maintaining the temperature at 25 °C. A non-enzymatic reaction was also performed at the same time to normalize the experimental values. All the reactions were performed in triplicates.

2.11. Enzyme kinetics

The kinetic parameters; Michaelis constant (K_m) and maximum velocity (V_{max}) for the glutathione S- transferase activity of rAbGST-θ were determined following Michaelis-Menten kinetics model. Varying concentrations of CDNB substrate (0.25–4 mM) with fixed concentrations of reduced GSH and *vice versa* were used according to the protocol described in section 2.10. The K_m and V_{max} values were determined using Lineweaver-Burk plot [40].

2.12. Temperature, pH, and inhibitor effect on rAbGST-θ activity

The effect of pH over rAbGST-θ activity was determined using a range of buffer series (pH: 3–11) while maintaining other factors as in section 2.10. CDNB was used as the specific substrate for these reactions. To evaluate the temperature effect over rAbGST-θ activity, water baths with various temperatures (10–60 °C) were used with CDNB substrate as specified in section 2.10. Cibacron blue (CB): a GST inhibitor was used to determine the inhibition of rAbGST-θ activity using various CB concentrations (0.001–100 μM) as described previously [41].

2.13. Disk diffusion assay

A disk diffusion assay was performed to compare the effectiveness of the persistence of untransformed *E. coli* (DE3), *E. coli* transformed with pMAL-c2X empty vector, and the AbGST-θ/pMAL-c2X construct over H_2O_2, $CdCl_2$, $CuSO_4$, and $ZnCl_2$, as described previously [42]. Briefly, 0.5 mM IPTG induced bacterial cultures were incubated at 25 °C for 4 h and then evenly spread on LB agar plates. Differentially treated Whatman filter-paper disks (30%: 5 μL of H_2O_2, 1 M $CdCl_2$, 1 M $CuSO_4$ and 1 M $ZnCl_2$) were placed on each agar plate. After an overnight incubation at 37 °C, the diameter of each clearance zone was measured and subjected for statistical analysis.

2.14. Statistical analysis

The data were reported with mean ± standard deviation (SD) while all the experiments were performed in triplicates. Significant difference between the groups were evaluated through the unpaired student's *t*-test. For the tissue distribution analysis and disk diffusion assay, one-way variance (ANOVA) with Duncan's Post Hoc multiple comparison was performed to analyze the significant differences within the groups. Statistical significance was considered according to the P-values less than 0.05 ($P < 0.05$).

3. Results

3.1. Molecular characterization of AbGST-θ

A nucleotide sequence of *GST-θ* was identified from our abalone transcriptome database, and sequence information was deposited in the NCBI GenBank under the accession number of: MK226199. The identified open reading frame (ORF) of *AbGST-θ* encoded a putative protein with 230 amino acids (aa) with a 26.6 kDa of molecular weight and 8.9 of theoretical iso electric point. The instability index was computed to be 40.73.

The AbGST-θ did not possess any signal peptides, as revealed from analysis with SignalP 4.1 software. According to the conserved domain analysis conducted with NCBI, AbGST-θ contained two soluble GST domains: A thioredoxin-like N-terminal domain (Residues 1–75), and a C- terminal domain (110–203). Eight G-sites at the positions of: S^{11}, Q^{12}, H^{40}, K^{41}, K^{52}, L^{53}, E^{66}, S^{67}, and one sulfate binding site (Q^{12}) were identified at the N- terminal of AbGST-θ. Moreover, ten H-sites were observed in the AbGST-θ C-terminal at: H^{104}, R^{108}, G^{109}, A^{112}, M^{113}, F^{115}, R^{116}, I^{120}, E^{174}, and Q^{177}. Furthermore, the motif scan analysis revealed that AbGST-θ consists of three casein kinase II phosphorylation sites (146–149; 165–168; 206–209) and two protein kinase C phosphorylation sites (192–194; 211–213).

3.2. Homology analysis of AbGST-θ

The pairwise sequence alignment analysis was carried out to compare the identity and similarity percentages of AbGST-θ with other known GST-θ homologues (Table 2). According to the observed data, the highest sequence identity and similarity was observed with

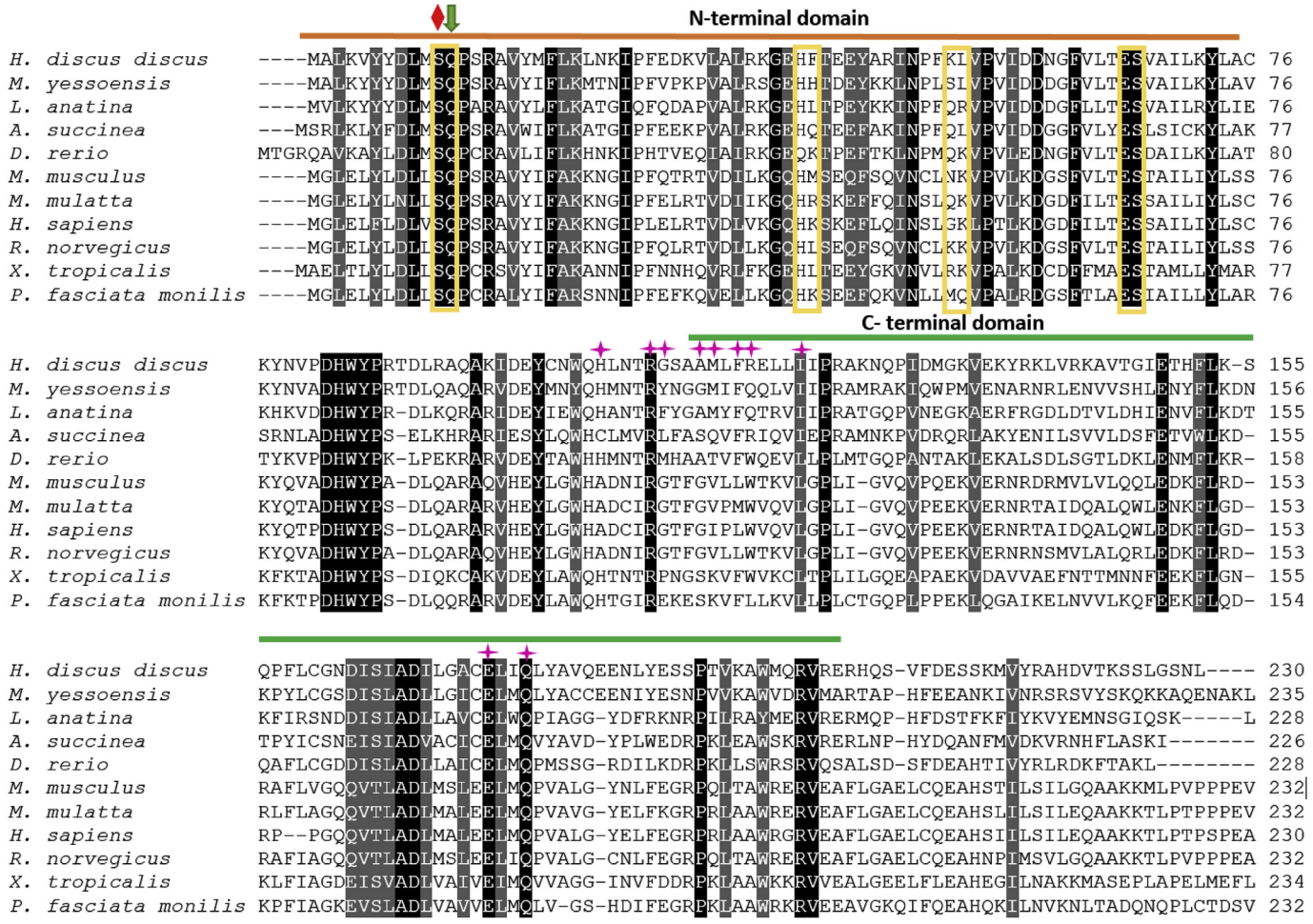

Fig. 1. Multiple sequence alignment of the amino acid sequences of AbGST-θ and its orthologs from different organisms. Fully conserved amino acids are shown in black, and strongly conserved and weakly conserved amino acids are shown in dark grey and light grey, respectively. The N-terminal domain and the C-terminal domain are marked with orange and green colored lines, respectively. The conserved Ser^{11} and sulfate binding site (Q^{12}) are marked with red and green color symbols, respectively. The putative G-sites are shown with yellow color boxes and the pink color symbols indicate the H-sites. (For interpretation of the references to color in this figure legend, the reader is referred to the Web version of this article.)

Mizuhopecten yessoensis (Japanese Weathervane Scallop) as 59.1% and 75.3%, respectively. The predicted multiple sequence alignment of AbGST-θ with other molluscan and non-molluscan organisms demonstrated that the N-terminal region is highly conserved through the evolution compared to the C-terminal region (Fig. 1.). Highly conserved GSH binding sites were observed in the N-terminal at S^{11}, Q^{12}, E^{66}, and S^{67} while substitutions were observed in H^{40}, F^{41}, K^{52}, and L^{53} positions. Of the C-terminal H-sites, R^{108}, E^{174}, and Q^{177} were highly conserved among all the species through the evolution, although H^{104}, G^{109}, A^{112}, M^{113}, F^{115}, R^{116}, and I^{120} sites exhibited replacements.

A phylogenetic tree was constructed for AbGST-θ together with other various GST classes, using the neighbor joining method (Fig. 2.). According to the figure, GST-θ had formed a separate clade including evolutionary different organisms together. However, AbGST-θ clearly clustered together with molluscan GST-θ: *Mizuhopecten yessoensis* and *Crassostrea gigas*. Separate sub clades were observed for other GST classes, and previously identified disk abalone (*Haliotis discus discus)* GSTs had been appropriately placed in the respective classes.

3.3. Illustration of AbGST-θ structural model

In order to analyze the structural features of AbGST-θ, a three-dimensional model was constructed using Swiss-Modelling and analyzed with PyMOL computer software (Fig. 3A). N- terminal and C-terminal domains could be identified separately which were connected to each other via a short tract. The N-terminal domain consisted of a βαβ unit connected to a ββα unit via a surface exposed region which contains two small α-helices. The structural topology of the C-terminal domain consisted of only six α-helices. The orange colored sphere represents the Ser^{11} residue which is considered a characteristic feature in GST- θ class. The surface representations of human GST- θ (Fig. 3 B, D) and AbGST-θ (Fig. 3C, E) demonstrates the highlighted C-terminal tail in red color. According to the figure, human GST- θ showed a long C-terminal extension compared to AbGST-θ. The blue color surface represents the H-site, and the green color surface represents the G-site region in both figures.

3.4. Tissue specific distribution analysis

To evaluate the tissue specific distribution of *AbGST-θ* and its various physiological functions, mRNA transcriptions were determined from disk abalone hemocytes, gills, mantles, digestive tracts, adductor muscles, and hepatopancreases (Fig. 4.). The highest expression level was observed from the digestive tract (~26 fold), followed by hepatopancreases (~20 fold). All the examined tissues had expressed *AbGST-θ* differently, indicating their potential physiological roles within the body.

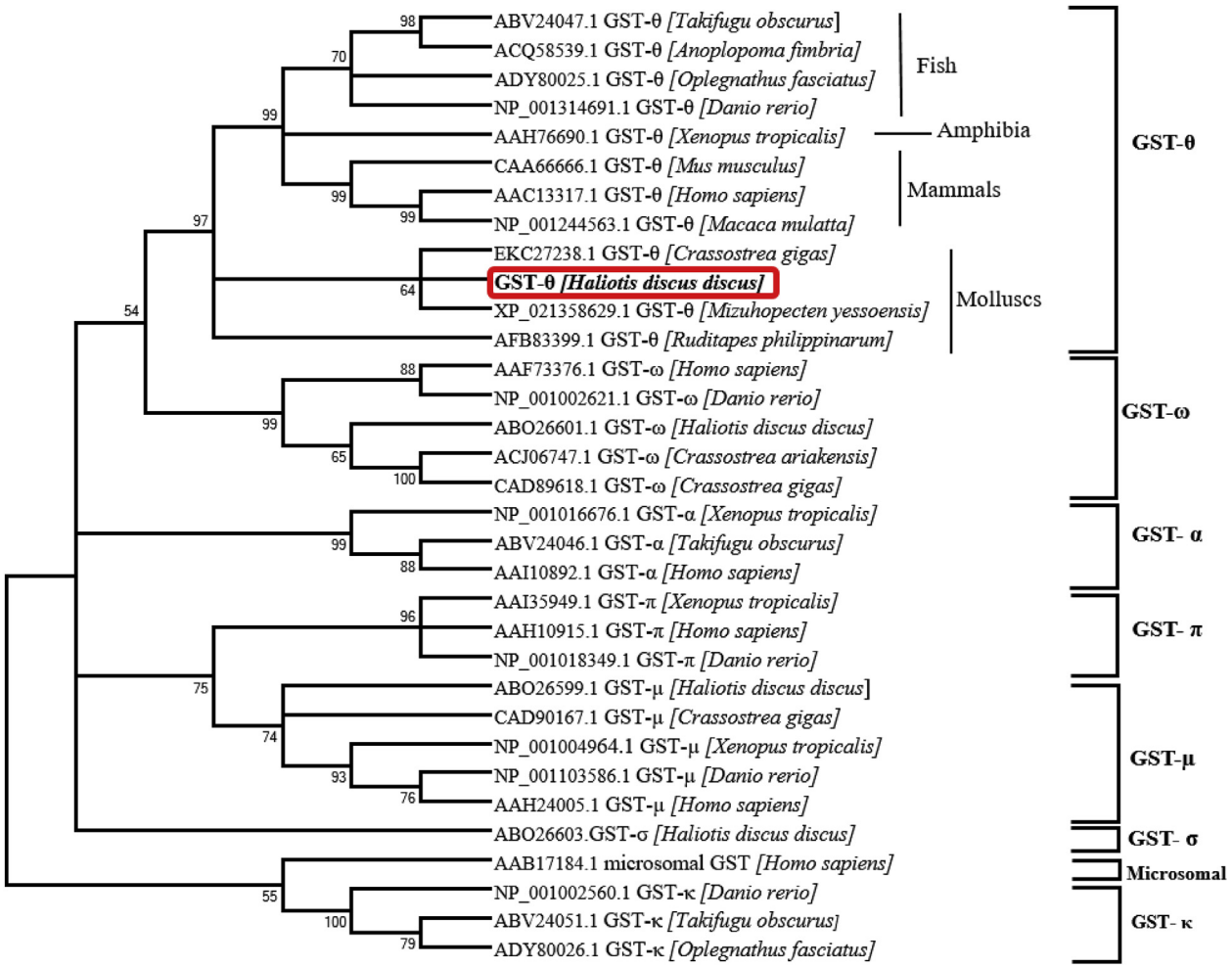

Fig. 2. A phylogenetic tree constructed using the neighbor-joining method based on different classes of GSTs. The bootstrap values are shown at the node of each branch. The NCBI accession numbers are given with the organism name.

3.5. Expression analysis of AbGST-θ after challenge experiment

In vivo time-course challenge experiments with LPS, *V. parahaemolyticus,* and poly I:C were carried out to determine the temporal variations of *AbGST-θ* gene expressions in gills (Fig. 5 A, B, C) and hemocytes (Fig. 5 D, E, F). The *AbGST-θ* was significantly upregulated after 48 h (~4-fold) p.i. of LPS in abalone gills (Fig. 5A). Meanwhile the poly I:C injection was able to significantly upregulate *AbGST-θ* in abalone gill tissue at 48 h (~5-fold) of p.i. (Fig. 5B). Furthermore, *V. parahaemolyticus* injection resulted in significant upregulations in abalone gill tissue at 24 h (~2-fold) and 72 h (~3-fold) of p.i (Fig. 5C).

The mRNA expression of *AbGST-θ* was significantly upregulated at 72 h and 120 h p.i. of LPS and *V. parahaemolyticus* in hemocytes (Fig. 5D and F). Moreover, poly I:C stimulation significantly upregulated the expression of *AbGST-θ* only at 72 h of p.i (Fig. 5E).

3.6. Induced protein expression and purification of rAbGST-θ

The CDS of AbGST-θ was cloned in to pMAL-c2X expression vector, and over expressed in *E. coli* BL21 (DE3) bacterial strain. The recombinant MBP-tagged fusion protein was purified from IPTG-induced cells using amylose affinity chromatography system. SDS-PAGE analysis was performed using protein fractions obtained from various purification steps throughout the process (Fig. 6.). No protein induction was observed in the uninduced cells. The resultant AbGST-θ/MBP fusion protein exhibited a band of ~70 kDa, which is compatible with the predicted molecular mass of AbGST-θ-26.6 kDa; MBP 42.5 kDa.

3.7. Functional characterization of rAbGST-θ

3.7.1. Biochemical properties of rAbGST-θ

The GSH conjugating catalytic activity of rAbGST-θ towards different substrates as CDNB, DCNB, 4-NBC, 4-NPB, and ECA were measured and shown in Table 3. It showed the highest catalytic activity towards the CDNB substrate (5.38 ± 0.09 μmol min $^{-1}$ mg $^{-1}$) with detectable activities towards 4-NBC (2.516 ± 0.08 μmol min $^{-1}$ mg $^{-1}$) and ECA (0.521 ± 0.07 μmol min $^{-1}$ mg $^{-1}$) substrates. No detectable activities were observed for DCNB and 4-NPB substrates. All the assays were performed for MBP alone, and no detectable catalytic activity was observed. Thus, it is considered that MBP may not significantly affect the enzymatic properties of fusion rAbGST-θ.

Using CDNB as the specific substrate, the optimum pH and temperature for maximum catalytic activity of rAbGST-θ were determined (Table 4). The optimum pH was detected as pH: 7.5 while giving highest activities within a narrow range from pH 7 to 9 (Fig. 7A). The optimum temperature of rAbGST-θ for CDNB conjugation activity was ~37 °C (Fig. 7B). Moreover, the higher temperatures resulted in the loss of enzymatic activities. Furthermore, 100% inhibition of rAbGST-θ-CDNB conjugation activity was observed with 100 μM concentration of CB (Fig. 7C). The IC_{50} value for CB was calculated as 0.08 ± 0.01 μM.

3.7.2. Enzyme kinetics

The rAbGST-θ enzyme activity was measured with different concentrations of CDNB and GSH. With a fixed concentration of CDNB, the K_m and V_{max} were calculated as 5.21 ± 0.22 mM and

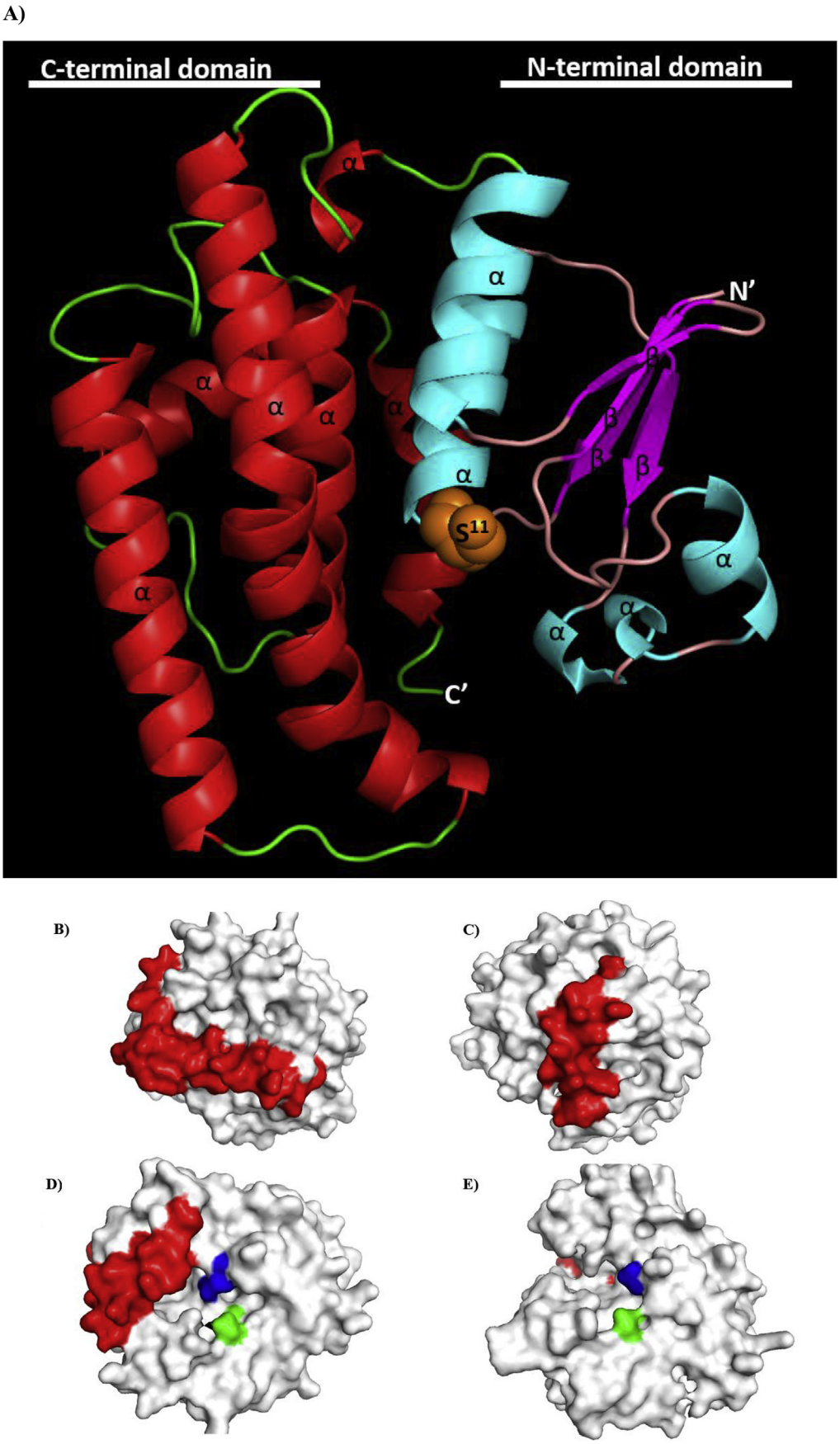

Fig. 3. A) Predicted three-dimensional structure of AbGST-θ. The α-helices and β-sheets are marked, and the orange colored sphere represents the Ser^{11} residue which is considered as a characteristic feature in GST- θ class. Surface representations of human GST-θ (B, D) and AbGST-θ (C, E) highlighting the C-terminal tails in red. The blue colored surface represents the H-site and green colored surface represents the G-site region in each figure. The 3D structure models were predicted using the Swiss-model server and visualized using PyMOL software. (For interpretation of the references to color in this figure legend, the reader is referred to the Web version of this article.)

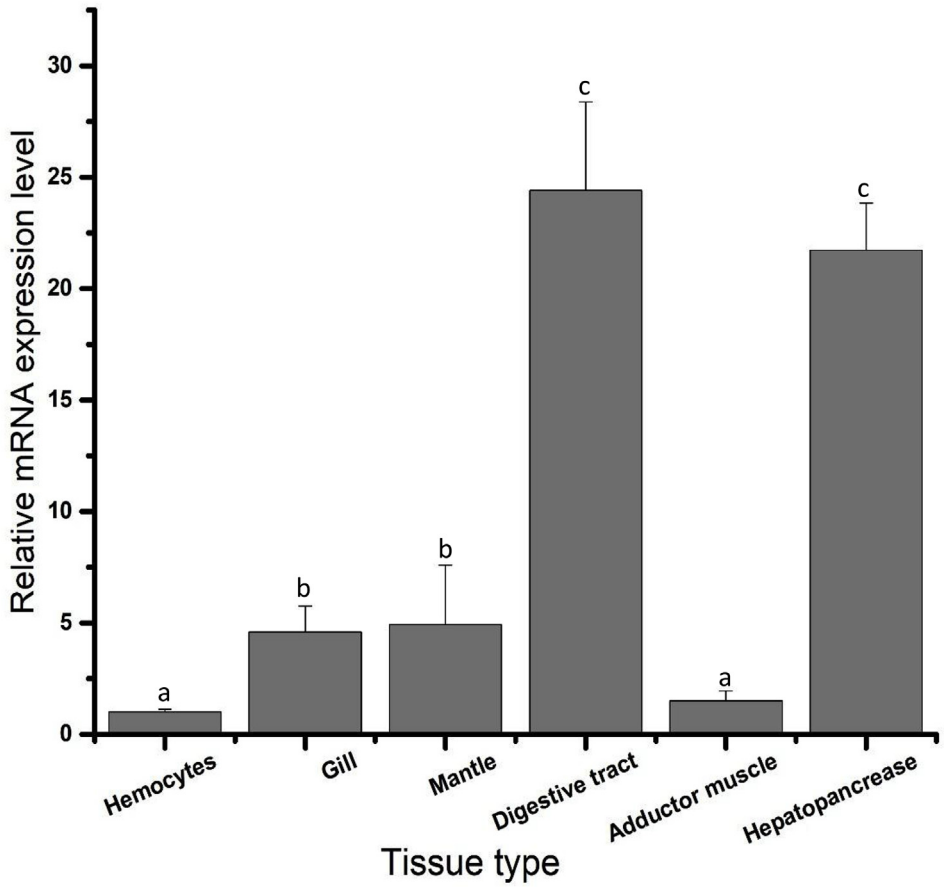

Fig. 4. Tissue specific transcriptional profile of *AbGST-θ*. Data are presented as mean ± standard deviation (n = 3). Significant differences within each group were analyzed using a one-way analysis of variance (ANOVA) with Duncan's Post Hoc multiple comparisons test. Data indicated with different letters are significantly different ($p < 0.05$) within the group.

10.68 ± 0.10 μmol min $^{-1}$ mg $^{-1}$, respectively. Meanwhile with a fixed concentration of GSH, the K_m and V_{max} values were calculated as 2.65 ± 0.18 mM and 8.23 ± 0.09 μmol min $^{-1}$ mg $^{-1}$, respectively (Table 4).

3.7.3. Disk diffusion assay

Clearance zones with various diameters were observed around all the H_2O_2 treated disks. Among them, the largest clearance zone was observed at the untransformed *E. coli* plate while the other two were smaller than this (Supplementary fig. 1). Apart from that, all the heavy metal treated disks also exhibited clearance zones with different diameters. Maximum diameters for $CdCl_2$, $ZnCl_2$, and $CuSO_4$ treatments were observed in the untransformed *E. coli* plates, whereas the AbGST-θ transformed plates showed significantly smaller clearance zones around the disks (Fig. 8.).

4. Discussion

Most of the cytosolic GSTs are available in nature as dimers, with a varying subunit molecular mass of 23 kDa–27 kDa [43]. The predicted molecular weight of AbGST-θ (26.6 kDa) was agreed with other previously identified theta class GSTs [11,44]. Furthermore, the absence of signal peptides within AbGST-θ indicated it may be a cytosolic protein [45].

All GSTs contain the same basic protein structure with two distinct N-terminal and C-terminal domains consisting of G-sites and H-sites, respectively [46]. NCBI-CDD analysis verified this, as the presence of N-terminal and C-terminal domains in AbGST-θ were exhibited. According to the multiple sequence alignment, the N-terminal region can be determined as highly conserved, while expressing more diversification in the C-terminal region. The G-sites in the N-terminal domain are involved in the maintenance of a high affinity for GSH, while H-sites in the C-terminal domain are responsible for increasing the capability of enzymes in detoxifying high amounts of substrates [46]. The C- terminal variability indicates the diversification in the substrate specificity of the enzyme within the class towards xenobiotics [43]. Altogether, these binding sites contribute to the catalytic activities of GSTs by forming multifunctional dimeric forms. The presence of H-site residues: G^{109}, A^{112}, M^{113}, F^{115}, and I^{120} were identified as hydrophobic residues contributing to the hydrophobic nature of the protein surface. This hydrophobic nature is required for the binding of hydrophobic electrophiles. Moreover, theta class possess a conserved Ser residue at their N-terminal, instead of Tyr residue in other GSTs (α, π, μ) which is a unique feature of GST- θ [47]. This Ser^{11} residue is involved in the enzyme activation [47]. However, it was stated that any mutation in this Ser^{11} residue has experienced an enzyme inactivation, therefore it is highly conserved among the theta class members [47]. Thereby, the presence of Ser^{11} in AbGST-θ confirms its classification as a member of theta class GST and allows the possession of proper enzyme activities in it. Compared with the surface representation of human GST-θ with AbGST-θ, it is possible to identify a long extension of C-terminal tail in human GST-θ [48]. This explains the differences of GSH binding affinity of mammalian and non-mammalian GST-θ [48] as this extended C-terminal tail together with adjacent H-site can block the GSH binding site in mammals. However, non-mammalian GST-θ possess very deep but accessible G-sites in their structure [48] as already indicated from our study. Therefore, it is possible to expect a high affinity of GSH binding activity from AbGST-θ compared with human GST-θ, according to structural analysis.

The primary structural analysis of AbGST-θ showed higher sequence similarities with other invertebrate and vertebrate orthologues (> 53%). This allowed the suggestion that GST-θ had been relatively conserved through the evolution among all the analyzed organisms. Nonetheless, the maximum identity and similarity of AbGST-θ could be

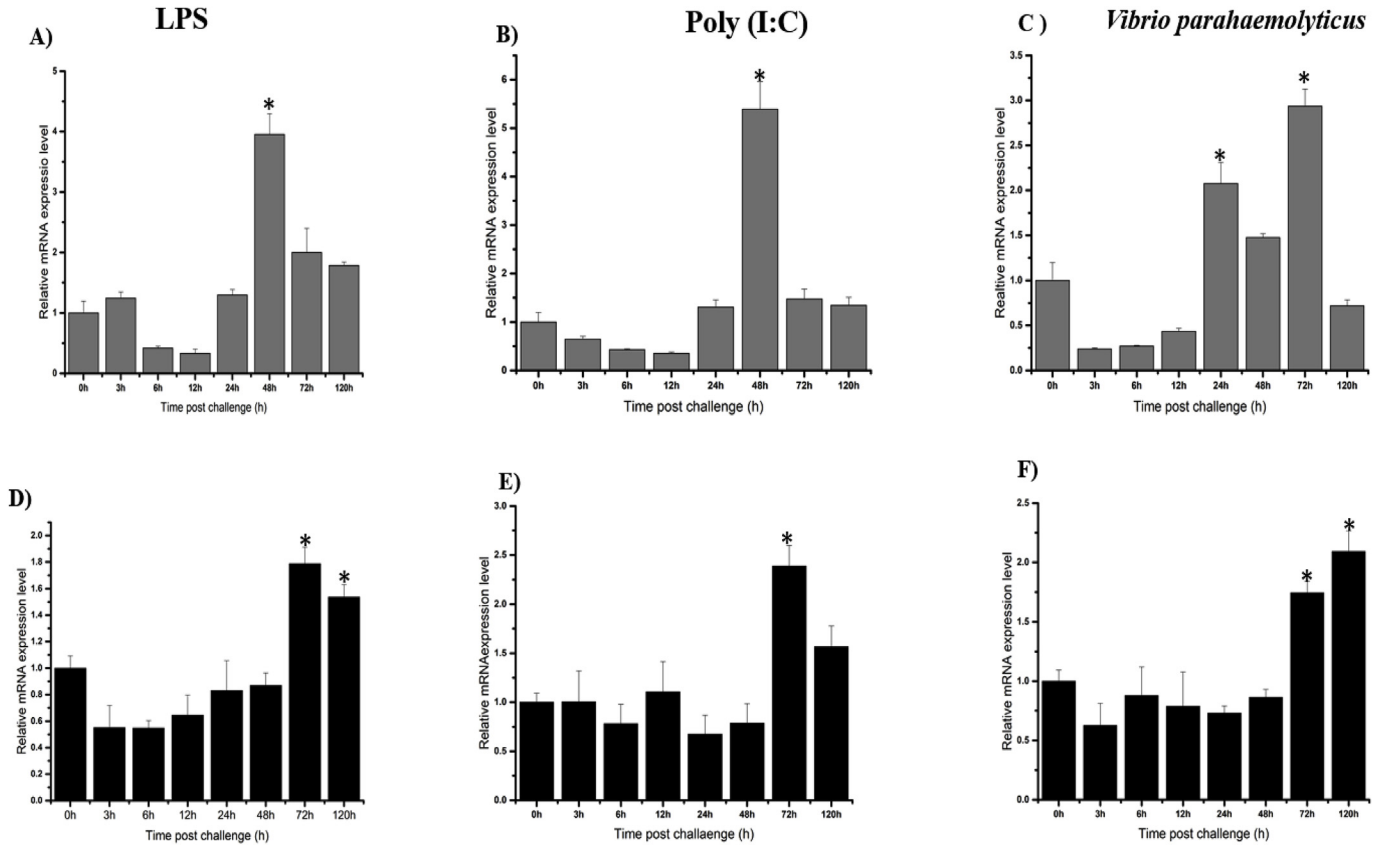

Fig. 5. Relative mRNA expression, analyzed by qPCR of *AbGST-θ* over time in gill tissues (A, B, C), and hemocytes (D, E, F) in response to challenges with LPS (A, D), poly I:C (B, E), and *Vibrio parahaemolyticus* (C, F). Data are presented as mean ± standard deviation (n = 3). Data marked with an * represent a statistical difference in expression compared with the 0 h post-injection baseline.

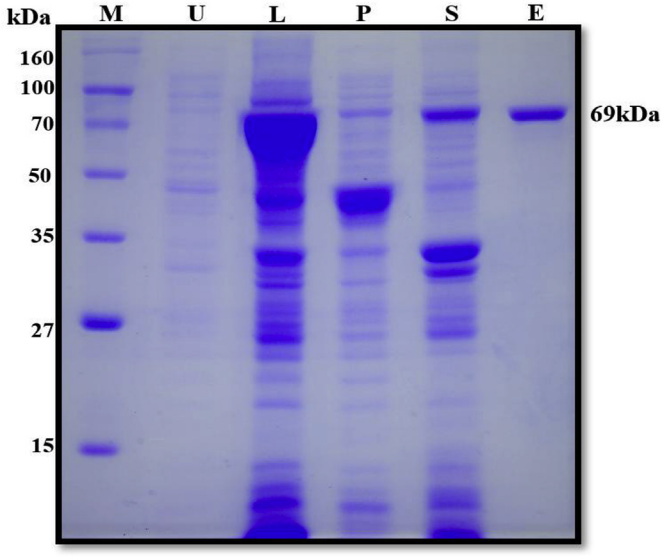

Fig. 6. SDS-PAGE analysis of purified rAbGST-θ. M: protein marker, U: un-induced extract, L: lysate from IPTG induced cells, P: pellet from IPTG induced cells, S: supernatant from IPTG induced cells, E: purified recombinant protein after elution.

observed from the molluscan orthologues indicating their evolutionary relatedness with the phylum Mollusca. Although the marine GSTs are not well classified at present, in this study it is possible to define a relationship for AbGST-θ with other previously identified GST-θ enzymes using the constructed phylogenetic tree.

Table 3
Substrate specific parameters at 25 °C, when the substrate and GSH concentrations were 1.0 mM each, and the specific activities of AbGST-θ towards the different substrates.

Substrate	pH	λ_{max} (nm)	Molecular extinction Coefficient (ε) (mM $^{-1}$ cm $^{-1}$)	Specific activity (μmol min $^{-1}$ mg $^{-1}$)
CDNB	6.5	340	9.6	5.38 ± 0.09
DCNB	7.5	345	8.5	n.d
4-NPB	6.5	310	1.2	n.d
4-NBC	6.5	310	1.9	2.52 ± 0.08
ECA	6.5	270	5.0	0.52 ± 0.07

n.d – not detected.

The level of GSTs expressions in different tissues showed significant variations due to number of factors as identified in earlier studies. For instance, sex of the organism, developmental stage, different tissue specific factors, and the type of xenobiotics in contact, are some of the factors which can modulate the regulation and expression of GSTs [11]. Moreover, these variations may have occurred due to the multiple functions of the GSTs [49]. Human *GST-θ* is expressed highly in kidney, liver, small intestine and in the brain [50]. In the hermaphroditic fish *Rivulus marmoratus, GST-θ* has given its higher expression in the liver, intestine, gonad, and in skin [51]. Apart from that, *GST-θ* from *Macrobrachium rosenbergii* was expressed highly in hepatopancreases and hemocytes [4]. Moreover, in *Apostichopus japonicus,* highest expression levels of *GST-θ* were observed in the intestine and respiratory tree [12]. As reported in a previous study on the Manila clam (*Ruditapes philippinarum*), *GST-θ* was highly expressed in hemocytes, gills, and in the mantle [11]. Furthermore, one recent study of disk abalone GST-κ

Table 4
Optimum temperature, pH, Michaelis-Menten kinetic parameters, and inhibitor IC_{50} values for AbGST-θ using CDNB as the substrate (n = 3).

Protein	Optimum Temperature (°C)	Optimum pH	Inhibitory IC $_{50}$ (μM)	Kinetics $CDNB_{(GSH(1mM))}$ $K_{m(mM)}$ V_{max} (μmol $mg^{-1}min^{-1}$)	Kinetics $GSH_{(CDNB(1mM))}$ $K_{m(mM)}$ V_{max} (μmol $mg^{-1}min^{-1}$)
AbGST-θ	37	7.5	0.08 ± 0.01	5.21 ± 0.22 10.68 ± 0.10	2.65 ± 0.18 8.23 ± 0.09

showed its higher expression in the mantle, digestive tract, and in muscles [52]. The highest expression of disk abalone *GST-θ* was observed in the digestive tract and hepatopancreases in this study. This, along with previous evidence, indicates the tissue-specific and isoform-specific manner of GSTs. Usually, various exogeneous and endogenous harmful compounds are directly in contact with the digestive tract of the aquatic animals. Furthermore, in mollusks, the digestive tract is one of the main organs involved in the accumulation and detoxification of toxins, as well as the immune defense, and metabolic and homeostatic regulation [53]. Therefore, the digestive tract should be equipped with free radical scavengers to mediate the high level of ROS produced during oxidative respiration [54]. Glutathione (GSH) is identified with its antioxidant potentials in cells, which are regulated and controlled by GSTs in different cellular compartments [54]. At the same time, GSTs are capable enough to detoxify various other electrophilic xenobiotics such as environmental pollutants [55]. Therefore, it is possible to have high amount of *AbGST-θ* in the digestive tract of the disk abalone, as we have observed in this study, to maintain an effective detoxification system for the host. Moreover, hepatopancreases are closely in contact with the food digestion process of the organisms, and in invertebrates they work as a functional analogue to the liver in vertebrates [56]. Therefore, it is required that hepatopancreases contain high levels of detoxification enzymes, and thus we may have obtained a higher expression of *AbGST-θ* in disk abalone hepatopancreases.

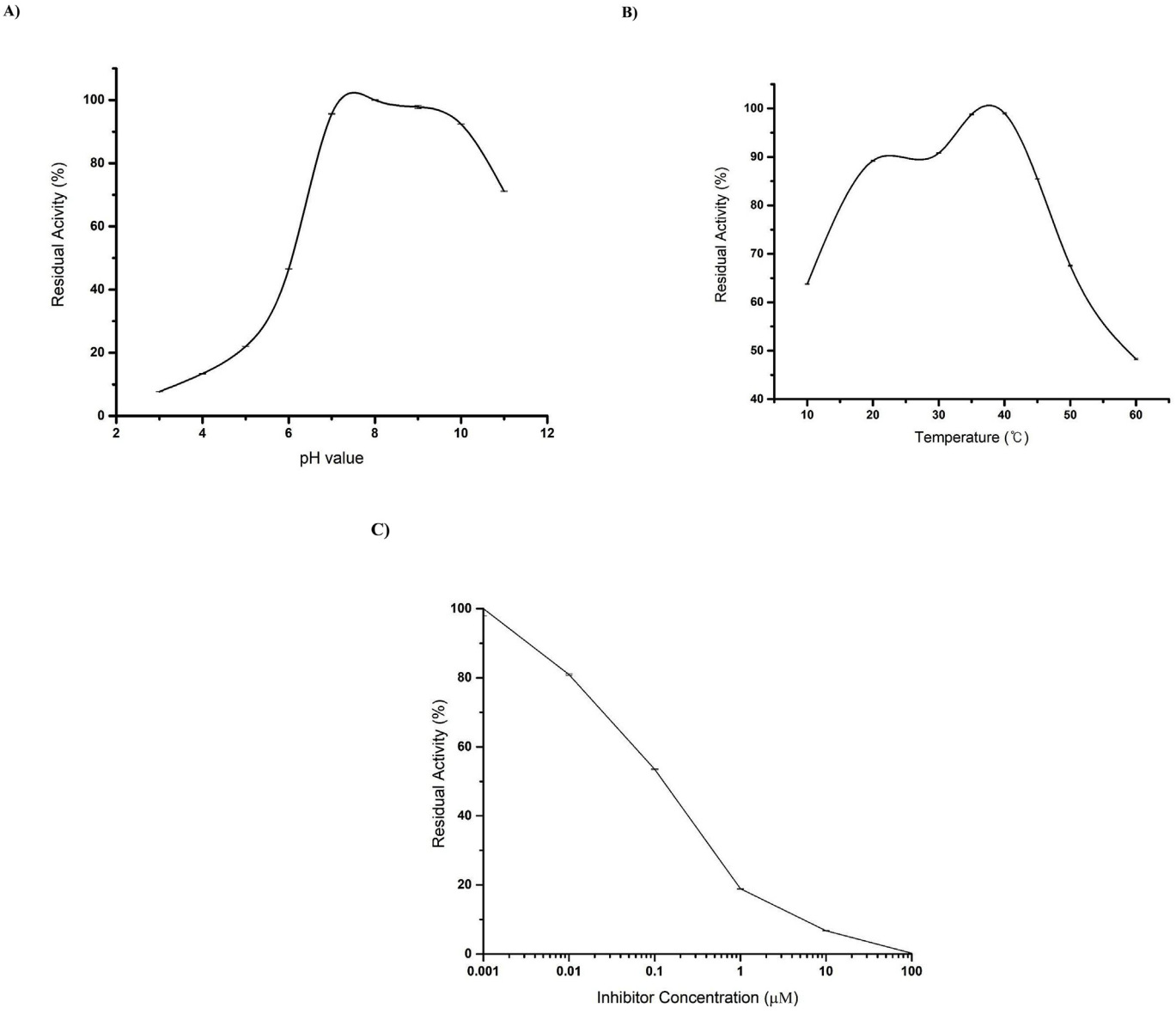

Fig. 7. A) The effect of pH, B) temperature and C) inhibitor (Cibacron Blue) concentration on the GSH conjugating activity of AbGST-θ.

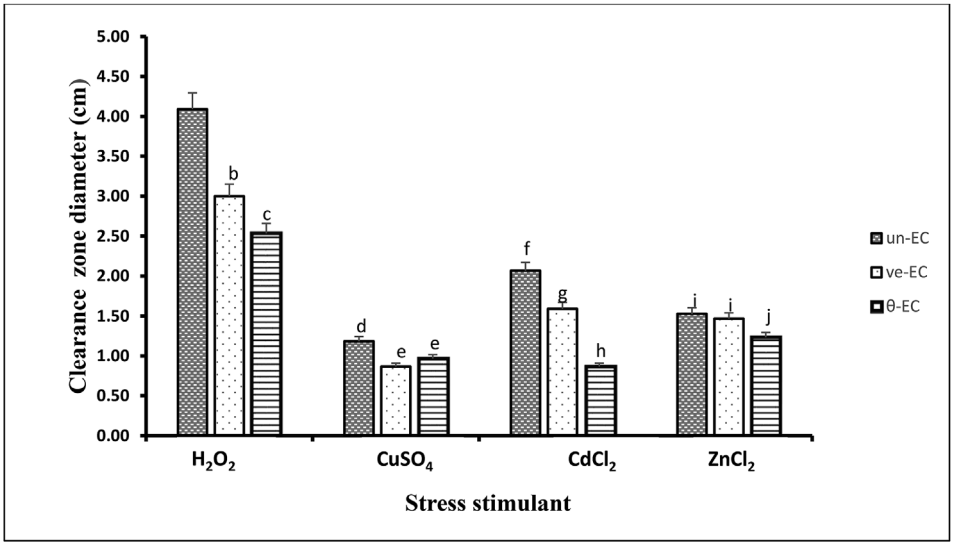

Fig. 8. Disk diffusion assay of AbGST-θ against *E. coli* BL21. The diameter of the clearance zone (cm) was measured in plates with un-transformed *E. coli* (un-EC), *E. coli* transformed with the pMALc2X vector (ve-EC), and *E. coli* transformed with the AbGST-θ/pMAL-c2X vector (θ-EC). Disks were impregnated with H_2O_2, $CdCl_2$, $CuSO_4$, and $ZnCl_2$. Data are presented as mean ± standard deviation (n = 3). Significant differences within each group were analyzed using a one-way analysis of variance (ANOVA) with Duncan's Post Hoc multiple comparisons test. Data indicated with different letters are significantly different ($p < 0.05$) within the group.

Living in a continuously dynamic aquatic environment, abalones are highly exposed to different types of pathogens and harmful substances. In order to evaluate the mRNA expression patterns of *AbGST-θ* over different immune stimulants, qPCR analysis was performed using the synthesized cDNA from disk abalones challenged with LPS, poly (I:C), and *Vibrio parahaemolyticus*. *V. parahaemolyticus* is identified as a highly pathogenic Gram-negative bacterium for disk abalones, being the causative agent of withering syndrome [18]. It has resulted in mass mortalities of the post-larval stage of abalone cultures, causing a high economic loss [15]. Abalone gills covered with epidermal mucus are directly in contact with sea water. They are therefore required to possess a resistance over the pathogens present in the sea water [57]. Moreover, various antioxidant and immune regulated genes in hemocytes have exhibited significant variations in their expressions over pathogenic and environmental conditions [51,52]. Therefore, we selected gill and hemocytes as target sites to determine the immune responses of *AbGST-θ* upon various immune responses in this study.

GSTs are well known detoxification enzymes which act on several cytotoxic and genotoxic compounds in order to eliminate them from the cell by converting them in to harmless metabolites [6]. According to the results obtained from this current study, considerable variations of *AbGST-θ* expressions could be identified after challenging the abalones with above mentioned immune stimulants. The expression pattern variabilities are dependent on the time of post injection and the type of tissue. The observed temporal mRNA expression profiles of *AbGST-θ* indicate that the modulation of *AbGST-θ* expressions are higher in gills (outer tissue) than in hemocytes (inner tissue). Same observations were reported from the study on the Manila clam *GST-θ* [11] proposing GSTs protective functions over pathogens. In this study, we have observed significant elevations of *AbGST-θ* in gills earlier than that of the hemocytes. It has been suggested that GSTs may have the ability to act as a signaling molecule to the inner tissues, which passes the alerts of danger or information on damaged cell destruction [11]. The free circulatory hemocytes allow the maintenance of different biological mechanisms together with immunological homeostasis [60]. As GSTs are phase II detoxification enzymes, a high elevation of their expression in various challenging environments allows the protection of the host upon different toxicities [11,43,53]. Otherwise, their immune related roles were discovered by recent studies on mollusks [11,43,53], fish [32,55], and in mammals [10,63]. Significant differences in the immune system of mollusks have been observed among the classes in the same phylum and even within a species [63]. Due to the lack of work regarding the abalone immune system, the actual immune mechanisms to incorporate with bacterial, viral and parasitic infections may differ in abalones compared with other mollusks. Nonetheless, it was stated that pathogenic invasions may have the ability to increase the phagocytic activities within an organism [63] which produce ROS to kill the invading microorganisms. However, its over production can damage biomolecules, which may result in tissue injury and the destruction of tissue homeostasis [64]. To prevent and treat these cellular dysfunctions, neutralizing and eliminating of these by-products is required to protect the cells from the negative effects of the reactive oxygen intermediates [65]. A network of antioxidants including catalases, superoxide dismutase, glutathione reductases, glutathione peroxidase, thioredoxins, and GSTs are involved in regulating cellular ROS levels in an integrated manner [61]. Upon pathogenic invasion, the induction of GSTs has been experienced and explained as a result of elevated ROS levels generated by phagocytic respiratory burst, toxic lipid peroxidation products, organic hydroperoxides, and endotoxic products like LPS [61]. Moreover, GST transcription is triggered by ROS, once bound with the response element on the promoter [49]. Therefore, being a member of the GST superfamily, it is logical to expect anti-infection responses from *AbGST-θ* in order to combat various pathogens. Based on the results observed from this present study, we believe that due to pathogenic invasions, abalones may have activated their phagocytic and oxidative burst activities while producing an excess amount of ROS, which may cause oxidative stress. After eliminating the pathogen, *AbGST-θ* plays a protective role to reduce the excessive ROS from host cells and avoid oxidative damage. Therefore, by expressing significant upregulations over bacterial, LPS, and viral mimetic treatments, it has provided enough evidence to suggest the *AbGST-θ* innate immune response in host defensive mechanisms.

The characterization of rAbGST-θ specific activities over different substrates revealed the equivalent to pre-defined GST homologues [16,45]. The rAbGST-θ showed its highest activity towards the CDNB; an universal GST substrate, comparable with GST-θ homologues from the Manila clam [11] and silkworm [66], but in contrast with humans [3] and rats [67]. The contrasted results with human GST-θ is confirmed with the structural variations observed between mammalian and non-mammalian GST-θ, as described in the 3D structural analysis. However, no detectable activity of rAbGST-θ was observed towards the DCNB substrate comparable with mammalian [68] and molluscan [11] GST-θ homologues. Although the level of activity varies among different species, activation of rAbGST-θ towards predominantly halogenated aromatics suggests that rAbGST-θ possess the same substrate profile along with the GST-θ class enzymes from Manila clam and silk worm [16,63].

To analyze the catalytic properties of rAbGST-θ, Michaelis-Menten

kinetic parameters were determined. The V_{max} and K_m values for any molluscan GST-θ has not been determined to date. However, through the values obtained from the Lineweaver-Burk plot, rAbGST-θ showed relatively similar enzyme kinetic parameters along with Australian sheep blowfly [47], silkworm [66], and fish [51] with CDNB substrate.

Apart from that, rAbGST-θ showed their optimum CDNB conjugation activity at a higher temperature (~37 °C) proposing GST-θ high temperature adaptability, in line with the study of the Manila clam GST-θ [11]. Moreover, the CDNB: GSH conjugation activity of rAbGST-θ extended for a range of pH values. Early studies based on the Manila clam [11] reported a narrow pH range (5.5–6.5), which contrasts with our study. Collectively, having maximum activities of rAbGST-θ in a diverse range of temperature and pH, allows us to expect AbGST-θ mediated host defensive activity of abalones in a dynamic environment. For the determination of the inhibition of CDNB-GSH conjugating activity of rAbGST-θ, CB was used as a pre-defined GST inhibitor by previous studies [42,43]. The activity inhibition indicates the presence of a dinucleotide fold in the protein which facilitates the binding of CB to the protein, although this was challenged by the lack of inhibition by NAD^+ or $NADP^+$ [69].

In a biological system, oxidative stress can occur when the production of free radicals and ROS exceeds the antioxidant capacity of the cellular antioxidants. Disturbance of the balance between oxidants and antioxidants leads to tissue injury and DNA damage [70]. H_2O_2 is relatively stable ROS found in aerobic cells in a low concentration, which is generated as a byproduct of the cellular metabolism [71]. It has a significant ability of converting spontaneously in to highly reactive hydroxyl radicals (OH^-) which causes damage to the cell membrane, disturbs the structural integrity, and increases the cellular toxicity which may result in cell death [71]. Both soluble and MAPEG families of GSTs can reduce these compounds rendering them harmless [72]. Furthermore, they are capable of detoxifying downstream products of oxidative damage such as the reactive aldehydes 4-hydroxynoneal and acrolein [6]. Therefore, in our study, the ability of rAbGST-θ to reduce the negative effect of H_2O_2 was assessed from the disk diffusion assay, with the use of H_2O_2 as a stress generator. The results provide evidence for AbGST-θ's potential ability to efficiently overcome the harmful stress produced by H_2O_2.

In this study, we also determined the recovering ability of AbGST-θ to overcome the stress mounted by certain abundant heavy metals in the aquatic environment: Cd, Cu, and Zn. These heavy metals are released into the aquatic environment through natural and human mediated activities. Cd is identified as a toxic heavy metal for several aquatic species, which can influence their growth, behavior, and physiological functions [73]. Moreover, they have a high affinity over the thiol groups of the cysteine residues, and its replacement can result in protein disruption [73]. As Cu is an essential micronutrient of living organisms, an excessive amount can adversely affect on organism [74]. As it is a redox active metal, Cu can catalyze the production of ROS, which leads to oxidative stress [74]. Zinc is another essential heavy metal which is required for cell proliferation, differentiation, and apoptosis [75]. Nonetheless, early studies provide evidence for the induced oxidative stress caused by an excessive amount of Zn, which results in transcriptional changes of GSTs [53,68].

Among the various treatments, AbGST-θ showed strong protective ability towards the H_2O_2 induced oxidative stress. However, when comparing the diameter of the clearance zones, a significant protection ability of AbGST-θ was observed towards the stress caused by the excessive amounts of Zn and Cd in the host cells. Furthermore, the undefined margin in the clearance zone of $CdCl_2$ treated disks evidenced the retarded growth of the bacterial cells due to the Cd toxicity, as suggested in previous studies [41]. During the enzymatic detoxification process, being phase II enzymes, GSTs are responsible for catalyzing the conjugation of activated xenobiotics in to water soluble endogenous substrates, such as reduced GSH [76]. Several transport mechanisms are available for the elimination of these glutathione conjugates, such as ATP-dependent GS-x PUMP, multi specific organic anion transporters (MOAT), and a broad-specificity anion transporter of dinitrophenol S–GSH conjugates (Dnp-SG ATPase) [76]. According to the results obtained from our current study, evidence is provided for the detoxification and antioxidant activities of GST-θ from disk abalones over different heavy metals which are abundant in their environment, which is in line with previous studies [45,72,73]. However, the concentration of the heavy metal, duration of the exposure, and several other environmental factors may affect the recovery efficiency of abalones living in the natural environment.

5. Conclusion

In conclusion, *AbGST-θ* was identified and cloned in to pMAL-c2X expression vector and the recombinant protein was expressed and purified using the affinity chromatography method. Through the use of open access databases functional domains, conserved regions, and catalytic residues of AbGST-θ were determined. The enzymatic activities of the recombinant protein were determined using different substrates, which resulted in low affinities for CDNB and GSH substrates. The digestive tract and the hepatopancreas showed the highest tissue specific distribution for *AbGST-θ*. Expression profiles revealed the potential ability of AbGST-θ to respond over different immune stimulants. The protection ability of AbGST-θ over different heavy metals and oxidative stresses was assessed in the disk diffusion assay. Altogether, our findings for AbGST-θ support the classical explanation of the xenobiotic detoxification of GSTs, whilst providing evidence for the immunological host defense mechanism.

Acknowledgements

This research was supported by Golden Seed Project, Ministry of Agriculture, Food and Rural Affairs (MAFRA), Ministry of Oceans and Fisheries (MOF), Rural Development Administration (RDA) and Korea Forest Service (KFS) [213008-05-1-SB730].

Appendix A. Supplementary data

Supplementary data related to this article can be found at https://doi.org/10.1016/j.fsi.2019.04.004.

References

[1] R.S. Chhabra, Intestinal Absorption and Metabolism of Xenobiotics vol 33, (1979), pp. 61–69 December.
[2] C. Ioannides, 1 Xenobiotic Metabolism : an Overview vol 4, (1995), p. 2002. Toth.
[3] J.D. Hayes, D.J. Pulford, The glut athione S-transferase supergene family: regulation of GST and the contribution of the lsoenzymes to cancer chemoprotection and drug resistance Part I, Crit. Rev. Biochem. Mol. Biol. 30 (6) (Jan. 1995) 445–520.
[4] J. Arockiaraj, et al., A cytosolic glutathione s-transferase, GST-theta from freshwater prawn *Macrobrachium rosenbergii*: molecular and biochemical properties, Gene 546 (2) (2014) 437–442.
[5] N. Allocati, Glutathione Transferases : Substrates , Inihibitors and Pro-drugs in Cancer and Neurodegenerative Diseases, *Oncogenesis*, 2018.
[6] J.D. Hayes, J.U. Flanagan, I.R. Jowsey, Glutathione transferases, Annu. Rev. Pharmacol. Toxicol. 45 (1) (2005) 51–88.
[7] S.R. Kasthuri, et al., Genomic characterization, expression analysis, and antimicrobial function of a glyrichin homologue from rock bream, *Oplegnathus fasciatus*, Fish Shellfish Immunol. 35 (5) (2013) 1406–1415.
[8] X. Ji, P. Zhang, R.N. Armstrong, G.L. Gilliland, The three-dimensional structure of a glutathione S-transferase from the mu gene class. Structural analysis of the binary complex of isoenzyme 3-3 and glutathione at 2.2-Å resolution, Biochemistry 31 (42) (1992) 10169–10184.
[9] N. Motoyama, W.C. Dauterman, Purification and properties of housefly glutathione S-transferase, Insect Biochem. 7 (4) (1977) 361–369.
[10] S. Landi, Mammalian class theta GST and differential susceptibility to carcinogens: a review, Mutat. Res. Rev. Mutat. Res. 463 (3) (2000) 247–283.
[11] K. Saranya Revathy, N. Umasuthan, Y. Lee, C.Y. Choi, I. Whang, J. Lee, "First molluscan theta-class Glutathione S-Transferase: identification, cloning, characterization and transcriptional analysis post immune challenges," *Comp*, Biochem. Physiol. - B Biochem. Mol. Biol. 162 (1–3) (2012) 10–23.
[12] Y. Shao, et al., Molecular cloning and functional characterization of theta class

glutathione S-transferase from Apostichopus japonicus, Fish Shellfish Immunol. 63 (2017) 31–39.
[13] P.A. Cook, The worldwide abalone industry, Sci. Res. (December) (2014) 1181–1186.
[14] D.R. Livingstone, Organic Xenobiotic Metabolism in Marine Invertebrates vol 7, (1991).
[15] J. Cai, J. Li, K.D. Thompson, C. Li, H. Han, Isolation and characterization of pathogenic Vibrio parahaemolyticus from diseased post-larvae of abalone *Haliotis diversicolor* supertexta, J. Basic Microbiol. 47 (1) (2007) 84–86.
[16] K.K. Lee, P.C. Liu, C.Y. Huang, *Vibrio parahaemolyticus* infectious for both humans and edible mollusk abalone, Microb. Infect. 5 (6) (2003) 481–485.
[17] P.C. Liu, Y.C. Chen, C.Y. Huang, K.K. Lee, Virulence of *Vibrio parahaemolyticus* isolated from cultured small abalone, *Haliotis diversicolor* supertexta, with withering syndrome, Lett. Appl. Microbiol. 31 (6) (2000) 433–437.
[18] I. Zorrilla, et al., Vibrio species isolated from diseased farmed sole, *Solea senegalensis* (Kaup), and evaluation of the potential virulence role of their extracellular products, J. Fish Dis. 26 (2) (2003) 103–108.
[19] M. Cardinaud, et al., *Vibrio harveyi* adheres to and penetrates tissues of the European abalone *Haliotis tuberculata* within the first hours of contact, Appl. Environ. Microbiol. 80 (20) (2014) 6328–6333.
[20] D. Pichon, et al., Characterization of abalone *Haliotis tuberculata-Vibrio harveyi* interactions in gill primary cultures, Cytotechnology 65 (5) (2013) 759–772.
[21] J. Cai, H. Han, Z. Song, C. Li, J. Zhou, Isolation and Characterization of Pathogenic *Vibrio Alginolyticus* from Diseased Postlarval Abalone , *Haliotis Diversicolor* Supertexta (Lischke), (2006), pp. 1222–1226.
[22] A.J. Hobday, M.J. Tegner, NOAA Technical Memorandum NMFS, (2000).
[23] P.T. Raimondi, C.M. Wilson, R.F. Ambrose, J.M. Engle, T.E. Minchinton, "Continued declines of black abalone along the coast of California : are mass mortalities related to El Niño events ? 242 (2002) 143–152.
[24] N. Umasuthan, S.D.N.K. Bathige, S.R. Kasthuri, Q. Wan, I. Whang, J. Lee, Two duplicated chicken-type lysozyme genes in disc abalone *Haliotis discus discus*: molecular aspects in relevance to structure, genomic organization, mRNA expression and bacteriolytic function, Fish Shellfish Immunol. 35 (2) (2013) 284–299.
[25] D.A.S. Elvitigala, R.G.P.T. Jayasooriya, I. whang, J. Lee, First report on the gastropod proapoptotic AIF3 counterpart from disk abalone (*Haliotis discus discus*) deciphering its transcriptional modulation by induced pathogenic stress, Fish Shellfish Immunol. 47 (2) (2015) 697–705.
[26] M. Droege, B. Hill, The Genome Sequencer FLX^{TM} System-Longer reads, more applications, straight forward bioinformatics and more complete data sets, J. Biotechnol. 136 (1–2) (2008) 3–10.
[27] C.J.A. Sigrist, et al., New and continuing developments at PROSITE, Nucleic Acids Res. 41 (D1) (2013) 344–347.
[28] T.N. Petersen, S. Brunak, G. von Heijne, H. Nielsen, SignalP 4.0: discriminating signal peptides from transmembrane regions, Nat. Methods 8 (10) (2011) 785–786.
[29] K. Tamura, D. Peterson, N. Peterson, G. Stecher, M. Nei, S. Kumar, MEGA5: molecular evolutionary genetics analysis using maximum likelihood, evolutionary distance, and maximum parsimony methods, Mol. Biol. Evol. 28 (10) (2011) 2731–2739.
[30] H. McWilliam, et al., Analysis tool web services from the EMBL-EBI, Nucleic Acids Res. 41 (Web Server issue) (2013) 597–600.
[31] F. Sievers, et al., Fast, scalable generation of high-quality protein multiple sequence alignments using Clustal Omega, Mol. Syst. Biol. 7 (1) (2014) 539–539.
[32] T. Schwede, J. Kopp, N. Guex, M.C. Peitsch, SWISS-MODEL: an automated protein homology-modeling server, Nucleic Acids Res. 31 (13) (2003) 3381–3385.
[33] W. DeLano, Pymol: an open-source molecular graphics tool, CCP4 Newsl. Protein Crystallogr. 700 (2002).
[34] A.F. Page, The MIQE guidelines and assessment of nucleic acids prior to qPCR and RT-qPCR, Therm. Sci. (2010) 1–3.
[35] Q. Wan, I. Whang, C.Y. Choi, J.S. Lee, J. Lee, "Validation of housekeeping genes as internal controls for studying biomarkers of endocrine-disrupting chemicals in disk abalone by real-time PCR," *Comp*, Biochem. Physiol. - C Toxicol. Pharmacol. 153 (3) (2011) 259–268.
[36] K.J. Livak, T.D. Schmittgen, "Analysis of relative gene expression data using real-time quantitative PCR and the $2-\Delta\Delta CT$ method, Methods 25 (4) (2001) 402–408.
[37] A. Alexandrov, K. Dutta, S.M. Pascal, MBP fusion protein with a viral protease cleavage site: one-step cleavage/purification of insoluble proteins, Biotechniques 30 (6) (2001) 1194–1198.
[38] M.M. Bradford, A rapid and sensitive method for the quantitation of microgram quantities of protein utilizing the principle of protein-dye binding, Anal. Biochem. 72 (1–2) (1976) 248–254.
[39] R.H. Michel, P.E. McGovern, The first, J. Biol. Chem. 249 (8) (1974) 7130–7139.
[40] J.D. Pollack, Enzyme Analysis 104 (1998).
[41] J.D.H.E. Jayasinghe, S.D.N.K. Bathige, B.H. Nam, J.K. Noh, J. Lee, Comprehensive characterization of three glutathione S-transferase family proteins from black rockfish (*Sebastes schlegelii*), Comp. Biochem. Physiol. C Toxicol. Pharmacol. 189 (2016) 31–43.
[42] Y.M. Lee, et al., Sequence, biochemical characteristics and expression of a novel Sigma-class of glutathione S-transferase from the intertidal copepod, *Tigriopus japonicus* with a possible role in antioxidant defense, Chemosphere 69 (6) (2007) 893–902.
[43] B. Blanchette, X. Feng, B.R. Singh, Review 9 (February) (2007) 513–542.
[44] S.D.N.K. Bathige, et al., Comparative Biochemistry and Physiology , Part C A mu class glutathione S-transferase from Manila clam *Ruditapes philippinarum* (RpGST μ): cloning , mRNA expression , and conjugation assays, Comp. Biochem. Physiol., C 162 (2014) 85–95.
[45] P. Talmud, L. Lins, R. Brasseur, "Prediction of signal peptide functional properties : a study of the orientation and angle of insertion of yeast invertase mutants and human apolipoprotein B signal peptide variants, 9 (4) (1996) 317–321.
[46] R.N. Armstrong, Structure, catalytic mechanism and evolution of the glutathione transferases, Chem. Res. Toxicol. 96 (2–18) (1997).
[47] P.G. Board, M. Coggan, M.C.J. Wilcet, M.W. Parkert, Evidence for an essential serine residue in the active site of the Theta class glutathione transferases, 250 (1995) 247–250.
[48] J. Rossjohn, et al., Human theta class glutathione transferase: the crystal structure reveals a sulfate-binding pocket within a buried active site, Structure 6 (1998) 309–322.
[49] Q. Wan, I. Whang, J. Lee, Molecular cloning and characterization of three sigma glutathione S-transferases from disk abalone (*Haliotis discus discus*), Comp. Biochem. Physiol. B Biochem. Mol. Biol. 151 (3) (2008) 257–267.
[50] P. Chandra, "Glutathione S-Transferases : a Brief on Classification and Gstm1-T1 Activity," No. January, (2017).
[51] Y.M. Lee, J.S. Seo, S.O. Jung, I.C. Kim, J.S. Lee, Molecular cloning and characterization of θ-class glutathione S-transferase (GST-T) from the hermaphroditic fish *Rivulus marmoratus* and biochemical comparisons with α-class glutathione S-transferase (GST-A), Biochem. Biophys. Res. Commun. 346 (3) (2006) 1053–1061.
[52] W.M.G. Sandamalika, T.T. Priyathilaka, D.S. Liyanage, S. Lee, H.K. Lim, J. Lee, Molecular characterization of kappa class glutathione S-transferase from the disk abalone (*Haliotis discus discus*) and changes in expression following immune and stress challenges, Fish Shellfish Immunol. 77 (March) (2018) 252–263.
[53] I. Marigómez, M. Soto, M.P. Cajaraville, E. Angulo, L. Giamberini, Cellular and subcellular distribution of metals in molluscs, Microsc. Res. Tech. 56 (5) (2002) 358–392.
[54] F.S. Ataya, et al., Genomics, phylogeny and in silico analysis of mitochondrial glutathione S-transferase-kappa from the camel *Camelus dromedarius*, Res. Vet. Sci. 97 (1) (2014) 46–54.
[55] B. Chen, et al., Genomic Analysis of Glutathione S-transferases 49 (4) (2017) 1437–1448.
[56] C.A. Contreras-Vergara, C. Harris-Valle, R.R. Sotelo-Mundo, G. Yepiz-Plascencia, A mu-class glutathione S-transferase from the marine shrimp *Litopenaeus vannamei*: molecular cloning and active-site structural modeling, J. Biochem. Mol. Toxicol. 18 (5) (2004) 245–252.
[57] Guilan Di, Types and distribution of mucous cells of the abalone *Haliotis diversicolor*, Afr. J. Biotechnol. 11 (37) (2012) 9127–9140.
[60] N. Cochennec-Laureau, M. Auffret, T. Renault, A. Langlade, Changes in circulating and tissue-infiltrating hemocyte parameters of European flat oysters, *Ostrea edulis*, naturally infected with *Bonamia ostreae*, J. Invertebr. Pathol. 83 (1) (2003) 23–30.
[61] N. Umasuthan, K. Saranya Revathy, Y. Lee, I. Whang, C.Y. Choi, J. Lee, A novel molluscan sigma-like glutathione S-transferase from Manila clam, *Ruditapes philippinarum*: cloning, characterization and transcriptional profiling, Comp. Biochem. Physiol. C Toxicol. Pharmacol. 155 (4) (2012) 539–550.
[63] C. Hooper, R. Day, R. Slocombe, J. Handlinger, K. Benkendorff, Stress and immune responses in abalone: limitations in current knowledge and investigative methods based on other models, Fish Shellfish Immunol. 22 (4) (2007) 363–379.
[64] B. Halliwell, Phagocyte-derived reactive species: salvation or suicide? Trends Biochem. Sci. 31 (9) (2006) 509–515.
[65] J.A. Knight, Review: free radicals, antioxidants, and the immune system, Ann. Clin. Lab. Sci. 30 (2) (2000) 145–158.
[66] K. Yamamoto, P. Zhang, F. Miake, N. Kashige, Y. Aso, Cloning , expression and characterization of theta-class glutathione S -transferase from the silkworm, Bombyx mori 141 (2005) 340–346.
[67] J.M. Harris, D.J. Meyer, B. Coles, B. Ketterer, A novel glutathione transferase (13-13) isolated from the matrix of rat liver mitochondria having structural similarity to class theta enzymes, Biochem. J. 278 (1991) 137–141.
[68] K.L. Tan, P.G. Board, Purification and characterization of a recombinant human Theta-class glutathione transferase (GSTT2-2), Biochem. J. 315 (1996) 727–732.
[69] M. Kalim Tahir, C. Guthenberg, B. Mannervik, Inhibitors for distinction of three types of human glutathione transferase, FEBS Lett. 181 (2) (1985) 249–252.
[70] C.H. Coyle, L.J. Martinez, M.C. Coleman, D.R. Spitz, N.L. Weintraub, K.N. Kader, Mechanisms of H2O2-induced oxidative stress in endothelial cells, Free Radic. Biol. Med. 40 (2006) 2206–2213.
[71] S.S.K. Wijeratne, S.L. Cuppett, V. Schlegel, Hydrogen peroxide induced oxidative stress damage and antioxidant enzyme response in Caco-2 human colon cells, J. Agric. Food Chem. 53 (22) (2005) 8768–8774.
[72] P.J. Sherratt, J.D. Hayes, 9 Glutathione S-Transferases vol 4, (2002).
[73] G. Bertin, D. Averbeck, Cadmium: cellular effects, modifications of biomolecules, modulation of DNA repair and genotoxic consequences (a review), Biochimie 88 (11) (2006) 1549–1559.
[74] T.C. Thounaojam, et al., Excess copper induced oxidative stress and response of antioxidants in rice, Plant Physiol. Biochem. 53 (2012) 33–39.
[75] M. Hambidge, N.F. Krebs, Zinc metabolism and requirements, Food Nutr. Bull. 22 (2) (2001) 126–132.
[76] D. SHEEHAN, G. MEADE, V.M. FOLEY, C.A. DOWD, Structure, function and evolution of glutathione transferases: implications for classification of non-mammalian members of an ancient enzyme superfamily, Biochem. J. 360 (1) (2001) 1–16.